

Full counting statistics of phonon-assisted Andreev tunneling through a quantum dot coupled to normal and superconducting leads

Bing Dong, G. H. Ding, and X. L. Lei

*Key Laboratory of Artificial Structures and Quantum Control (Ministry of Education),
Department of Physics and Astronomy, Shanghai Jiaotong University,
800 Dongchuan Road, Shanghai 200240, China and*

Collaborative Innovation Center of Advanced Microstructures, Nanjing, China

(Dated: August 13, 2018)

We present a theoretical investigation for the full counting statistics of the Andreev tunneling through a quantum dot (QD) embedded between superconducting (SC) and normal leads in the presence of a strong on-site electron-phonon interaction using nonequilibrium Green function method. For this purpose, we generalize the dressed tunneling approximation (DTA) recently developed in dealing with inelastic tunneling in a normal QD system to the Andreev transport issue. This method takes account of vibrational effect in evaluation of electronic tunneling self energy in comparison with other simple approaches and meanwhile allows us to derive an explicit analytical formula for the cumulant generating function at the subgap region. We then analyze the interplay of polaronic and SC proximity effects on the Andreev reflection spectrum, current-voltage characteristics, and current fluctuations of the hybrid system. Our main findings include: (1) no phonon side peaks in the linear Andreev conductance; (2) a negative differential conductance stemming from the suppressed Andreev reflection spectrum; (3) a novel inelastic resonant peak in the differential conductance due to phonon assisted Andreev reflection; (4) enhancement or suppression of shot noise for the symmetric or asymmetric tunnel-coupling system respectively.

PACS numbers: 74.70.-b, 74.45.+c, 71.38.-k, 72.70.+m, 74.78.Na

I. INTRODUCTION

Modern nanotechnology has facilitated the fabrication of single-electron devices using organic molecules. Since single molecule has much smaller mechanical parameters than semiconductor materials, it is very easy to excite the internal vibrational degrees of freedom (phonon modes) when electrons are incident upon the single molecule through a tunnel junction.¹⁻⁴ This has led to experimental observations of a variety of intriguing effects in the transport properties of the single-molecule transistors, for instance, the phonon-assisted current steps in the current-voltage characteristics of a variety of individual molecule connected to metal electrodes,¹⁻³ the Franck-Condon (FC) blockade in the current steps and negative differential conductance (NDC) due to nonequilibrated phonon excitation in the device of a suspended single-wall carbon nanotube.⁴ These experiments have stimulated great interest in theoretical investigations on electronic transport through a quantum dot (QD) connected to two electrodes subject to a local strong electron-phonon interaction (EPI).⁵⁻²²

In experiments, a QD embedded in superconducting (SC) and normal electrodes has attracted intensive studies for over decades, since this setup provides one of the most appropriate benchmarks to investigate the interplay between electron correlation and SC proximity-induced on-dot pairing effects, for example, in the experimental studies of the Kondo-enhanced Andreev transport,²³⁻²⁵ Andreev bound states,²⁶ and Cooper pair splitting.²⁷ Very recently, a carbon nanotube QD has been successfully connected to a Nb SC and a normal metal con-

tact and its subgap transport properties have been measured, leading to the observation of the phonon assisted resonant Andreev tunneling.²⁸ Actually, this interplay between electron-phonon correlation and SC pairing effects has been theoretically studied in literature,²⁹⁻³³ and predicted recently to be useful in ground-state cooling of a mechanical oscillator.³⁴ Based on the nonequilibrium Green function (NGF) method and the Lang-Firsov transformation, two simple decoupling approaches have been developed to examine the subgap transport in the polaronic regime: the single-particle approximation (SPA)^{29,32,33} and the polaron tunneling approximation (PTA).³¹

However, the two simple schemes are not able to give the electronic spectral density properly for the N-QD-N system, since both of them take no account of the vibrational effect on electronic self-energies due to tunneling in their calculations of the electronic GF.²² Besides, the two simple schemes have some other drawbacks. For instance, both of them predicted appearances of phonon side peaks in the conductance G with varying the gate voltage ε_d even in the zero bias voltage limit, which is inconsistent with the experiment results.^{1,5,12,21} We would like to see in the following of this paper that those studies for the N-QD-S system based on the two schemes inherit this unphysical result. Moreover, the SPA is not a current conservation approximation. While the PTA is albeit a current conservation approximation, it only considers the elastic scattering processes during electron tunneling.²¹

Fortunately, an advanced scheme over the SPA and PTA has recently been developed to overcome these drawbacks successfully, in which the vibrational effect has been taken into account in the calculation of elec-

tronic self-energies.²¹ This dressed tunneling approximation (DTA) is therefore believed to be able to give the electronic spectral function of a EPI system properly, and corrects the pathologies of SPA and PTA in the low-energy and high-energy regimes respectively.²² This scheme also predicts the correct transport behavior in the linear regime, no phonon side peaks in the G - ε_d curve. Moreover, the DTA fulfills the current conservation condition automatically and includes the inelastic tunneling processes naturally.²¹ The most great advantage of this nonperturbative scheme is that it allows us to obtain an explicit analytical expression for the full counting statistics (FCS) of inelastic electron tunneling in the strong EPI system.²¹ It is therefore very interesting to examine the interplay of the EPI and SC correlation effects on the FCS of electronic Andreev tunneling in the subgap regime using the DTA. It is indeed the purpose of the present paper.

The rest of the paper is organized as follows. In Sec. II, we present our model of the N-QD-S system and discuss the theoretical derivation for the FCS in the subgap transport regime in absence and presence of EPI, respectively. In both cases, the explicit analytical expressions of the FCS, current, and zero-frequency shot noise are derived. In Sec. III, we then present and analyze our numerical calculations for the electronic Andreev reflection spectrum, linear and nonlinear Andreev conductances, and shot noise, followed by a brief summary in Sec. IV.

II. MODEL AND THEORETICAL FORMULATION

A. Model Hamiltonian

To investigate the vibrational assisted electron tunneling in the N-QD-S system, we consider the simplest QD model in which a single electronic level is coupled to a localized vibrational mode, and is also coupled to a normal metal and a SC lead. The model Hamiltonian is

$$H = H_{QD} + H_N + H_S + H_{TN} + H_{TS}, \quad (1a)$$

with

$$H_{QD} = \varepsilon_d \sum_{\sigma} [d_{\sigma}^{\dagger} d_{\sigma} + g_{ep} d_{\sigma}^{\dagger} d_{\sigma} (a^{\dagger} + a)] + \omega_0 a^{\dagger} a, \quad (1b)$$

$$H_N = \sum_{\mathbf{k}\sigma} \varepsilon_{N\mathbf{k}} c_{N\mathbf{k}\sigma}^{\dagger} c_{N\mathbf{k}\sigma}, \quad (1c)$$

$$H_S = \sum_{\mathbf{k}\sigma} \varepsilon_{S\mathbf{k}} c_{S\mathbf{k}\sigma}^{\dagger} c_{S\mathbf{k}\sigma} + \sum_{\mathbf{k}} (\Delta c_{S\mathbf{k}\downarrow}^{\dagger} c_{S-\mathbf{k}\uparrow}^{\dagger} + \text{H.c.}), \quad (1d)$$

$$H_{TN} = \sum_{\mathbf{k}\sigma} (\gamma_N e^{-i\lambda(t)/2} c_{N\mathbf{k}\sigma}^{\dagger} d_{\sigma} + \text{H.c.}), \quad (1e)$$

$$H_{TS} = \sum_{\mathbf{k}\sigma} (\gamma_S c_{S\mathbf{k}\sigma}^{\dagger} d_{\sigma} + \text{H.c.}). \quad (1f)$$

Here, d^{\dagger} (d) denotes the operator of an electron with spin σ and energy ε_d at the QD. a^{\dagger} (a) is phonon creation

(annihilation) operator for the vibrational mode with energy quanta ω_0 . g_{ep} is the EPI strength. $c_{\eta\mathbf{k}}^{\dagger}$ ($c_{\eta\mathbf{k}}$) is the creation (annihilation) operator of an electron with spin σ , momentum \mathbf{k} , and energy $\varepsilon_{\eta\mathbf{k}}$ in the normal lead $\eta = N$ or the SC lead $\eta = S$. The SC lead is assumed to be described by the BCS Hamiltonian with a SC gap Δ . γ_{η} describes the tunnel-coupling matrix element between the QD and lead η . The corresponding coupling strength is defined as $\Gamma_{\eta} = 2\pi \sum_{\mathbf{k}} |\gamma_{\eta}|^2 \delta(\omega - \varepsilon_{\eta\mathbf{k}})$, which is assumed to be independent of energy in the wide band limit. In order to calculate the FCS, an artificially measuring field $\lambda(t)$ is introduced with respect to the normal lead on the Keldysh contour (In this paper, we focus our attention on the tunneling and its fluctuation measured in the normal lead only, and we therefore assume that the bias voltage is applied to the normal electrode, i.e. $\mu_N = \mu + V$, $\mu_S = \mu$, and we set $\mu = 0$ at the equilibrium condition): $\lambda(t) = \lambda_- \theta(t) \theta(\mathcal{T} - t)$ on the forward path and $\lambda(t) = \lambda_+ \theta(t) \theta(\mathcal{T} - t)$ on the backward path (\mathcal{T} is the measuring time during which the counting field is non-zero and the counting field will be set to be opposite constants on the forward and backward Keldysh contour as $\lambda_- = -\lambda_+ = \lambda$ in the final derivation).³⁵ Throughout we will use natural units $e = \hbar = k_B = 1$.

Since we are interested in the case of strong EPI in this paper, it is convenient to eliminate the EPI term in the Hamiltonian Eq. (1a) by applying a nonperturbative Lang-Firsov canonical transformation, i.e. $\tilde{H} = e^S H e^{-S}$ with $S = g d^{\dagger} d (a^{\dagger} - a)$ ($g = g_{ep}/\omega_0$).³⁶ The transformed Hamiltonian reads

$$\tilde{H} = \tilde{H}_{QD} + H_N + H_S + \tilde{H}_{TN} + \tilde{H}_{TS}, \quad (2a)$$

$$\tilde{H}_{QD} = \tilde{\varepsilon}_d \sum_{\sigma} \tilde{d}_{\sigma}^{\dagger} \tilde{d}_{\sigma} + \omega_0 a^{\dagger} a, \quad (2b)$$

$$\tilde{H}_{TN} = \sum_{\mathbf{k}\sigma} (\gamma_N e^{-i\lambda(t)/2} c_{N\mathbf{k}\sigma}^{\dagger} \tilde{d}_{\sigma} X + \text{H.c.}), \quad (2c)$$

$$\tilde{H}_{TS} = \sum_{\mathbf{k}\sigma} (\gamma_S c_{S\mathbf{k}\sigma}^{\dagger} \tilde{d}_{\sigma} X + \text{H.c.}), \quad (2d)$$

where $\tilde{\varepsilon}_d = \varepsilon_d - \frac{g_{ep}^2}{\omega_0}$ is the shifted energy level of the QD by the polaronic binding energy. To simplify notation we still use ε_d to denote the shifted level in the following of the paper. $\tilde{d}_{\sigma} = d_{\sigma} X$ denotes the new Fermionic operator dressed by the polaronic shift operator X ,

$$X = e^{g(a - a^{\dagger})}. \quad (2e)$$

B. Adiabatic Potential for FCS

The transport problem in the N-QD-S system can be solved with the Keldysh NGF technique in the Nambu space, in which a mixture Fermion operator, $\tilde{\psi}_d = (\tilde{d}_{\uparrow}, \tilde{d}_{\downarrow})^T$, has to be introduced to describe electronic dynamics involving SC correlation. Accordingly, we must define the contour-ordered GF of the QD, $G_d(t, t') =$

$-i\langle T_C \tilde{\psi}_d(t) \tilde{\psi}_d^\dagger(t') \rangle$ (T_C denotes time ordering along the Schwinger-Keldysh contour), and the GF of the decoupled lead η , $g_{\eta\mathbf{k}}(t, t') = -i\langle T_C \psi_{\eta\mathbf{k}}(t) \psi_{\eta\mathbf{k}}^\dagger(t') \rangle$ with $\psi_{\eta\mathbf{k}} = (c_{\eta\mathbf{k}\uparrow}, c_{\eta-\mathbf{k}\downarrow}^\dagger)^T$, in the Nambu representation.

The focus of the present work is the FCS of the subgap Andreev transport in the hybrid tunneling junction, which can be obtained from the cumulant generating function (CGF) as a Keldysh partition function

$$\chi(\lambda) = \left\langle T_C e^{-i \int_C (\tilde{H}_{TN}(t) + \tilde{H}_{TS}(t)) dt} \right\rangle. \quad (3)$$

Following the procedure outlined in Ref. 35, the CGF is in turn related to the adiabatic potential $-i\mathcal{TU}(\lambda) = \ln \chi(\lambda)$, whose derivative in the counting field λ_- can be expressed as^{21,35}

$$\begin{aligned} \frac{\partial \mathcal{U}(\lambda)}{\partial \lambda_-} &= \left\langle \frac{\partial \tilde{H}_{TN}(t)}{\partial \lambda_-} \right\rangle \\ &= -\frac{i}{2} \sum_{\mathbf{k}\sigma} \left\langle \gamma_N e^{-i\lambda_-/2} c_{N\mathbf{k}\sigma}^\dagger(t) \tilde{d}_\sigma(t) - \text{H.c.} \right\rangle. \end{aligned} \quad (4)$$

Employing the counting field-dressed GFs defined above,

we can easily formulate the derivative of the adiabatic potential in the counting field as

$$\frac{\partial \mathcal{U}(\lambda)}{\partial \lambda_-} = \sum_{\mathbf{k}} \frac{\gamma_N^2}{2} \int d\omega \text{Tr}_N \left[\Lambda e^{-i\bar{\lambda}/2} G_d^{-+}(\omega, \lambda) g_{N\mathbf{k}}^{+-}(\omega) - \Lambda^\dagger e^{i\bar{\lambda}/2} g_{N\mathbf{k}}^{-+}(\omega) G_d^{+-}(\omega, \lambda) \right], \quad (5)$$

where

$$\Lambda = \begin{pmatrix} e^{-i\lambda} & 0 \\ 0 & -e^{i\lambda} \end{pmatrix}, \quad (6)$$

and $\text{Tr}_N[\dots]$ is the trace over the Nambu space.

C. Noninteracting case

First we derive the general form of the adiabatic potential $\mathcal{U}(\lambda)$ for a noninteracting N-QD-S system. In this case, what we need is the GF of the QD obtained from a counting field λ dressed version of the Dyson equation in the frequency space,

$$G_d^{-1}(\omega, \lambda) = \begin{pmatrix} \omega - \epsilon_d - \Sigma_{11}^{-+} - \Sigma_{11}^r & \Sigma_{11\lambda}^{-+} & -(\Sigma_{12}^{-+} + \Sigma_{12}^r) & \Sigma_{12\lambda}^{-+} \\ \Sigma_{11\lambda}^{+-} & -(\omega - \epsilon_d + \Sigma_{11}^{+-} - \Sigma_{11}^r) & \Sigma_{12\lambda}^{+-} & -(\Sigma_{12}^{+-} - \Sigma_{12}^r) \\ -(\Sigma_{21}^{+-} + \Sigma_{21}^r) & \Sigma_{21\lambda}^{+-} & \omega + \epsilon_d - \Sigma_{22}^{+-} - \Sigma_{22}^r & \Sigma_{22\lambda}^{+-} \\ \Sigma_{21\lambda}^{+-} & -(\Sigma_{21}^{+-} - \Sigma_{21}^r) & \Sigma_{22\lambda}^{+-} & -(\omega + \epsilon_d + \Sigma_{22}^{+-} - \Sigma_{22}^r) \end{pmatrix}, \quad (7)$$

where the electronic self-energies $\Sigma_{\alpha\beta\lambda}^{\pm\mp,r}$ ($\alpha, \beta = 1, 2$ are the Nambu indices) are stemming from the tunnel-coupling contributions of the electronic degree of freedom on the QD with both the normal and SC leads, $\Sigma_{\alpha\beta\lambda}^{\pm\mp,r} = \Sigma_{N\lambda, \alpha\beta}^{\pm\mp,r} + \Sigma_{S, \alpha\beta}^{\pm\mp,r}$,

$$\Sigma_{N\alpha\beta}^r = -i\frac{1}{2}\Gamma_N \delta_{\alpha\beta}, \quad (8a)$$

$$\Sigma_{N\lambda}^{-+} = i\Gamma_N \begin{pmatrix} f_N(\omega)e^{i\lambda} & 0 \\ 0 & [1 - f_N(-\omega)]e^{-i\lambda} \end{pmatrix}, \quad (8b)$$

$$\Sigma_{N\lambda}^{+-} = -i\Gamma_N \begin{pmatrix} [1 - f_N(\omega)]e^{-i\lambda} & 0 \\ 0 & f_N(-\omega)e^{i\lambda} \end{pmatrix}, \quad (8c)$$

$$\Sigma_{N\lambda}^{\pm\mp} = \Sigma_{N\lambda}^{\pm\mp} |_{\lambda=0}, \quad (8d)$$

and

$$\Sigma_S^r = -i\frac{1}{2}\Gamma_S \beta_S(\omega) \begin{pmatrix} 1 & -\frac{\Delta}{\omega} \\ -\frac{\Delta}{\omega} & 1 \end{pmatrix}, \quad (8e)$$

$$\Sigma_S^{\mp\pm} = \pm i\Gamma_S \Re \beta_S(\omega) \begin{pmatrix} 1 & -\frac{\Delta}{\omega} \\ -\frac{\Delta}{\omega} & 1 \end{pmatrix} f_S(\pm\omega), \quad (8f)$$

with

$$\beta_S(\omega) = \frac{|\omega|\theta(|\omega| - \Delta)}{\sqrt{\omega^2 - \Delta^2}} - i\frac{\omega\theta(\Delta - |\omega|)}{\sqrt{\Delta^2 - \omega^2}}, \quad (8g)$$

and the Fermi distribution function $f_\eta(\omega) = [e^{(\omega - \mu_\eta)/T} + 1]^{-1}$ at lead η .

It should be noticed that we write the GF Eq. (7) in the direct product space of the Keldysh and Nambu spaces. This is the reason that the GF has a 4×4 matrix form. Simply calculating the derivative of the GF Eq. (7) with respect to the counting field λ gives

$$\frac{d}{d\lambda} G_d^{-1}(\omega, \lambda) = \begin{pmatrix} 0 & -\Gamma_N f_N(\omega) e^{i\lambda} & 0 & 0 \\ -\Gamma_N [1 - f_N(\omega)] e^{-i\lambda} & 0 & 0 & 0 \\ 0 & 0 & 0 & \Gamma_N [1 - f_N(-\omega)] e^{-i\lambda} \\ 0 & 0 & \Gamma_N f_N(-\omega) e^{i\lambda} & 0 \end{pmatrix}. \quad (9)$$

Then we apply Jacobi's formula for the derivative of the determinant of a matrix

$$\frac{d}{d\lambda} \det(G_d^{-1}(\lambda)) = \text{Tr} \left[\text{adj}(G_d^{-1}(\lambda)) \frac{d}{d\lambda} G_d^{-1}(\lambda) \right], \quad (10)$$

to yield

$$\frac{1}{\det(G_d^{-1}(\omega, \lambda))} \frac{d}{d\lambda} \det(G_d^{-1}(\omega, \lambda)) = \text{Tr} \left[G_d(\omega, \lambda) \frac{d}{d\lambda} G_d^{-1}(\omega, \lambda) \right], \quad (11)$$

where $\text{Tr}[\dots]$ is the trace over the direct product space of the Keldysh and Nambu spaces, not over the Nambu space only as in Eq. (5). Utilizing Eq. (9) to perform the trace calculation of right hand side of the last equation, we can find that it is exactly equal to the integrand in the right hand side of Eq. (5). Then after integrating with respect to the counting field, we can obtain the general formula for the adiabatic potential

$$\mathcal{U}(\lambda) = i \int \frac{d\omega}{2\pi} \ln \left[\frac{\det(G_d^{-1}(\omega, \lambda))}{\det(G_d^{-1}(\omega, 0))} \right]. \quad (12)$$

This is a direct generalization of the Fredholm determinant of the CGF to the noninteracting system involving SC electrode.

In order to investigate the current and noise, we now have to calculate the determinants inside the logarithm in Eq. (12). It is not quite an easy task. However, considering that we will focus our attention on the electron tunneling only in the subgap region at temperature and bias voltage well below the SC gap, $T \ll \Delta$ and $V \ll \Delta$, in the present investigation, we can take $\Sigma_S^{\pm\mp} = 0$ in our following derivation. To the end, we can obtain the general form for the adiabatic potential for the subgap Andreev tunneling

$$\mathcal{U}_A(\lambda) = i \int \frac{d\omega}{2\pi} \ln \left\{ 1 + T_A(\omega) [(e^{i2\lambda} - 1) f_N f_{-N} + (e^{-i2\lambda} - 1) (1 - f_N) (1 - f_{-N})] \right\}, \quad (13)$$

with the shorthand notations $f_N = f_N(\omega)$ and $f_{-N} = f_N(-\omega)$, and the Andreev reflection probability $T_A(\omega) = \Gamma_N^2 |G_{12}^r(\omega)|^2$. It is found that the subgap FCS remains binomial form but with a double-charge transfer. From Eq. (13), we can distinguish the elementary processes of electronic tunneling in the subgap region: (i) two opposite-spin electrons having energies equally higher

and lower the chemical potential are respectively transmitted from the normal lead to the QD, and eventually enter into the SC lead to form a Cooper pair. The probability of this process is $P_+ = T_A(\omega) f_N f_{-N}$. In literature, this is considered as Andreev reflection that an electron incident from the normal lead with energy ω tunnels into the QD, and subsequently picks up an opposite-spin electron with energy $-\omega$ to create a Cooper pair into the SC lead and leads to a hole propagating back to the normal lead; (ii) the reverse process with a probability $P_- = T_A(\omega) (1 - f_N) (1 - f_{-N})$; (iii) no transmission happens with a probability $P_0 = 1 - P_+ - P_-$.

From Eq. (13) we can evaluate the current and noise for the Andreev tunneling, respectively, as

$$I_A = - \left. \frac{\partial \mathcal{U}_A}{\partial \lambda} \right|_{\lambda=0} = -2 \int \frac{d\omega}{2\pi} T_A(\omega) (1 - f_N - f_{-N}), \quad (14)$$

$$S_A = i \left. \frac{\partial^2 \mathcal{U}_A}{\partial \lambda^2} \right|_{\lambda=0} = 4 \int \frac{d\omega}{2\pi} [T_A(\omega) (1 - f_N - f_{-N} + 2f_N f_{-N}) - T_A^2(\omega) (1 - f_N - f_{-N})^2]. \quad (15)$$

The differential Andreev conductance g_A is obtained by differentiating I_A with respect V as

$$g_A = \frac{2e^2}{h} \frac{1}{T} \int d\omega T_A(\omega) [f_-(1 - f_-) + f_+(1 - f_+)], \quad (16)$$

with $f_{\pm} = [e^{(\omega \pm V)/T} - 1]^{-1}$. The noise S_A can be rewritten as the sum of the equilibrium noise (thermal noise) S_{th} and the nonequilibrium noise (shot noise) S_{sh} ,

$$S_A = \frac{4e^2}{h} \int d\omega \{ T_A(\omega) [f_-(1 - f_-) + f_+(1 - f_+)] + T_A(\omega) [1 - T_A(\omega)] (f_- - f_+)^2 \}. \quad (17)$$

It can therefore be realized that the generalized nonequilibrium Nyquist-Johnson (NNJ) relation becomes

$$g_A = \frac{1}{2T} (S_A - S_{sh}), \quad (18)$$

for the two-particle correlation tunneling in the subgap region (double-charge transfer is relevant), in comparison with the NNJ relation for the usual single-particle tunneling in the normal system, $g = \frac{1}{4T} (S - S_{sh})$.

D. Electron-phonon interaction system

Now we generalize our above discussion for the FCS of the Andreev tunneling to the strong EPI case. For

this purpose, we still need to evaluate the counting field λ dressed Dyson equation for the GF of the QD. In the limit of a weak tunnel-couplings, $\Gamma_\eta \ll \omega_0$, the GF $G_d(t, t')$ in the Nambu representation can be decomposed into a product of a pure electronic part $G_c(t, t') = -i\langle T_C \psi_d(t) \psi_d^\dagger(t') \rangle$ and a phononic part $K(t, t') = \langle T_C \mathcal{K}(t) \mathcal{K}^\dagger(t') \rangle$ (the Born-Oppenheimer adiabatic approximation),^{14,16,20–22}

$$G_{d\alpha\beta}(t, t') \approx G_{c\alpha\beta}(t, t') K_{\alpha\beta}(t, t'), \quad (19)$$

with $\psi_d = (d_\uparrow, d_\downarrow)^T$ and $\mathcal{K} = (X, X^\dagger)^T$.

Another approximation employed in this paper is that the vibrational mode is assumed to be always at the equilibrium state, which leads to³⁶

$$K_{11}^{\mp\pm}(t, t') = K_{22}^{\mp\pm}(t, t') = \exp\{-g^2 [n_B(1 - e^{\mp i\omega_0\tau}) + (n_B + 1)(1 - e^{\pm i\omega_0\tau})]\}, \quad (20a)$$

$$K_{12}^{\mp\pm}(t, t') = K_{21}^{\mp\pm}(t, t') = \exp\{-g^2 [n_B(1 + e^{\mp i\omega_0\tau}) + (n_B + 1)(1 + e^{\pm i\omega_0\tau})]\}, \quad (20b)$$

with the Bose distribution $n_B = (e^{\omega_0/T} - 1)^{-1}$ at the temperature T and $\tau = t - t'$. Using the identity $\exp(z \cos \theta) = \sum_{n=-\infty}^{\infty} I_n(z) \exp(in\theta)$, these correlation functions can be expanded in a power series in $\exp(\pm i\omega_0\tau)$

$$K_{11}^{\mp\pm}(t, t') = K_{22}^{\mp\pm}(t, t') = \sum_{n=-\infty}^{\infty} w_n e^{\pm in\omega_0\tau}, \quad (21a)$$

$$K_{12}^{\mp\pm}(t, t') = K_{21}^{\mp\pm}(t, t') = \sum_{n=-\infty}^{\infty} (-1)^n w_n e^{\pm in\omega_0\tau}, \quad (21b)$$

with

$$w_n = e^{-g^2(2n_B+1)} e^{n\omega_0/2T} I_n(2g^2 \sqrt{n_B(n_B+1)}), \quad (22)$$

where $I_n(x)$ is the n th Bessel function of complex argument. Therefore, in the Fourier domain the dressed GF $G_d(\omega, \lambda)$ of the QD can be expressed in terms of the pure

electronic GF $G_c(\omega, \lambda)$, which are all dependent on the counting field λ , as

$$G_{d11(22)}^{\mp\pm}(\omega, \lambda) = \sum_{n=-\infty}^{\infty} w_n G_{c11(22)}^{\mp\pm}(\omega \pm n\omega_0, \lambda), \quad (23a)$$

$$G_{d12(21)}^{\mp\pm}(\omega, \lambda) = \sum_{n=-\infty}^{\infty} (-1)^n w_n G_{c12(21)}^{\mp\pm}(\omega \pm n\omega_0, \lambda). \quad (23b)$$

In what follows, we derive the counting field dressed Dyson equation of the pure electronic GF of the QD, $G_c(\omega, \lambda)$, based on the transformed Hamiltonian \tilde{H} Eq. (2a). There are two ways in literature to deal with the exponential operators X and X^\dagger in the transformed tunneling Hamiltonian Eqs. (2c) and (2d).^{21,22} One is to simply ignore the polaronic operators and/or replace them with their respective expectation values, $\langle X \rangle$ and $\langle X^\dagger \rangle$, in deriving the equation of motion (EOM) of $G_c(\omega)$. Under this approximation, the electronic self-energy is stemming only from the tunnel-coupling between the QD and electrodes and no polaronic effect is considered. This approximation is believed to be valid only if the Fermi sea effect of electrodes can be neglected in the limit of extremely weak tunnel-coupling, and is consequently called single-particle approximation.¹⁴ The main drawback of the SPA is that it does not obey current conservation condition and underestimates the electronic spectral density in the case of a N-QD-N system at low frequencies. To overcome these disadvantages, an improved procedure has to be proposed to correctly describe the polaronic effect in tunneling processes, in which the Born-Oppenheimer decoupling approximation is invoked once again in the EOM of $G_c(\omega)$ to disentangle the polaronic operator and operators of reservoirs yielding vibrational dressed self-energies of electronic tunneling,²¹

$$\Sigma_{c\alpha\beta\lambda}^{\mp\pm}(t, t') = \Sigma_{\alpha\beta\lambda}^{\mp\pm}(t, t') K_{\beta\alpha}^{\mp\pm}(t', t). \quad (24)$$

In this end, we obtain the counting field dressed Dyson equation for $G_c(\omega, \lambda)$ in frequency domain,

$$G_c^{-1}(\omega, \lambda) = \begin{pmatrix} \omega - \varepsilon_d - \Sigma_{c11}^{-+} - \Sigma_{c11}^r & \Sigma_{c11\lambda}^{-+} & -(\Sigma_{c12}^{-+} + \Sigma_{c12}^r) & \Sigma_{c12\lambda}^{-+} \\ \Sigma_{c11\lambda}^{+-} & -(\omega - \varepsilon_d + \Sigma_{c11}^{+-} - \Sigma_{c11}^r) & \Sigma_{c12\lambda}^{+-} & -(\Sigma_{c12}^{+-} - \Sigma_{c12}^r) \\ -(\Sigma_{c21}^{-+} + \Sigma_{c21}^r) & \Sigma_{c21\lambda}^{-+} & \omega + \varepsilon_d - \Sigma_{c22}^{-+} - \Sigma_{c22}^r & \Sigma_{c22\lambda}^{-+} \\ \Sigma_{c21\lambda}^{+-} & -(\Sigma_{c21}^{+-} - \Sigma_{c21}^r) & \Sigma_{c22\lambda}^{+-} & -(\omega + \varepsilon_d + \Sigma_{c22}^{+-} - \Sigma_{c22}^r) \end{pmatrix}, \quad (25)$$

with $(\alpha \neq \beta)$

$$\Sigma_{c\alpha\alpha\lambda}^{\mp\pm}(\omega) = \sum_{n=-\infty}^{\infty} w_n \Sigma_{\alpha\alpha\lambda}^{\mp\pm}(\omega \pm n\omega_0), \quad (26a)$$

$$\Sigma_{c\alpha\beta\lambda}^{\mp\pm}(\omega) = \sum_{n=-\infty}^{\infty} (-1)^n w_n \Sigma_{\alpha\beta\lambda}^{\mp\pm}(\omega \pm n\omega_0), \quad (26b)$$

$$\Sigma_{c\alpha\beta}^{\pm\mp}(\omega) = \Sigma_{c\alpha\beta\lambda}^{\pm\mp}(\omega) |_{\lambda=0}. \quad (26c)$$

Moreover, the retarded self-energy in time domain can be defined in the usual way from the lesser and greater counterparts, $\Sigma_{c\alpha\beta}^r(\tau) = \theta(\tau)[\Sigma_{c\alpha\beta}^{+-}(\tau) - \Sigma_{c\alpha\beta}^{-+}(\tau)]$, and

thus its expression in frequency domain is

$$\Sigma_{c\alpha\beta}^r(\omega) = i \int \frac{d\omega'}{2\pi} \mathcal{P} \frac{\Sigma_{c\alpha\beta}^{+-}(\omega') - \Sigma_{c\alpha\beta}^{-+}(\omega')}{\omega - \omega'} + \frac{1}{2} [\Sigma_{c\alpha\beta}^{+-}(\omega) - \Sigma_{c\alpha\beta}^{-+}(\omega)]. \quad (27)$$

Here \mathcal{P} means principal value integral. It is noticed that the resultant self-energies $\Sigma_{c\alpha\beta}^r(\omega)$ of electronic tunneling are highly dependent on the applied bias voltage. While in the SPA these retarded self-energies are assumed to be equal to those in a noninteracting QD-lead system, Eqs. (8a) and (8e), which are irrelevant to the bias voltage. We will find in the following that this bias voltage dependence of self-energies has profound effect on the tunneling current and its fluctuation in the subgap region. It is clear that this voltage dependence is stemming from the polaronic effect, since the phononic propagator is included in calculation of the self-energies. That is why this approximation is named as dressed tunneling approximation.²² Two advantages of the DTA are that it satisfies the current conservation condition and gives correct spectral density at both low and high frequencies in a N-QD-N system.^{21,22}

Another advantage of the DTA is that, when we apply this approximation to investigate the FCS of vibronic assisted tunneling in the hybrid N-QD-S system, the general formula for the adiabatic potential of a noninteracting QD system, Eq. (12), is still applicable as long as the GF G_d is replaced by G_c ,

$$U(\lambda) = i \int \frac{d\omega}{2\pi} \ln \left[\frac{\det(G_c^{-1}(\omega, \lambda))}{\det(G_c^{-1}(\omega, 0))} \right]. \quad (28)$$

Focusing on the subgap tunneling, we can write the sub-

gap adiabatic potential, after lengthy calculations, in an explicit expression,

$$\mathcal{U}_A(\lambda) = i \int \frac{d\omega}{2\pi} \ln \left\{ 1 + \sum_{nm} w_n w_m T_A(\omega) \times [(e^{i2\lambda} - 1)f_{N+n}f_{-N+m} + (e^{-i2\lambda} - 1) \times (1 - f_{N-n})(1 - f_{-N-m})] \right\}, \quad (29)$$

with $f_{N\pm n} = f_N(\omega \pm n\omega_0)$ and $f_{-N\pm n} = f_N(-\omega \pm n\omega_0)$, and the vibrational dressed Andreev reflection probability

$$T_A(\omega) = \Gamma_N^2 |G_{c12}^r(\omega)|^2. \quad (30)$$

This explicit analytical expression Eq. (29) provides us a clear physical picture for an elementary phonon-assisted Andreev reflection process: an electron incident from the normal lead with energy ω absorbs (or emits) $n > 0$ ($n < 0$) phonon and tunnels into the QD, then picks up an electron with energy $-\omega$ to create a Cooper pair, and simultaneously emits (or absorbs) $m > 0$ ($m < 0$) phonon, finally becomes a hole to come back to the normal lead.

Moreover, this expression Eq. (29) allows us to derive the formulae of phonon-assisted Andreev tunneling current and its shot noise as follows:

$$I_A = - \frac{\partial U_A(\lambda)}{\partial(\lambda)} \Big|_{\lambda=0} = -2 \int d\omega \sum_{nm} w_n w_m T_A(\omega) \times [(1 - f_{N-n})(1 - f_{-N-m}) - f_{N+n}f_{-N+m}], \quad (31)$$

$$S_A = i \frac{\partial^2 U_A(\lambda)}{\partial \lambda^2} \Big|_{\lambda=0} = 4 \int d\omega \left(\sum_{nm} w_n w_m T_A(\omega) [(1 - f_{N-n})(1 - f_{-N-m}) + f_{N+n}f_{-N+m}] - \left\{ \sum_{nm} w_n w_m T_A(\omega) [(1 - f_{N-n})(1 - f_{-N-m}) - f_{N+n}f_{-N+m}] \right\}^2 \right). \quad (32)$$

From Eq. (31) the current can be separated as two contributions of elastic and inelastic parts, $I_A = I_{el} + I_{in}$, where the elastic current is

$$I_{el} = -2 \int d\omega w_0^2 T_A(\omega) (1 - f_N - f_{-N}). \quad (33)$$

III. RESULTS AND DISCUSSIONS

In this section, we perform numerical investigation of vibronic effect on Andreev reflection properties of a hy-

brid N-QD-S system at the subgap region, by calculating the tunneling current and its shot noise based on Eqs. (31) and (32). In numerical calculations, we set the SC gap $\Delta = 1$ as the energy unit and choose the Fermi levels of the two leads as the reference of energy $\mu_N = \mu_S = \mu = 0$ at equilibrium. We also set the phonon energy $\omega_0 = 0.2\Delta$, since numerical fits of the experimentally measured data for the I - V curves predict the vibrational frequency ranging from a few $100\mu\text{eV}$ to a few meV and a strong EPI $g \leq 1$ for suspended carbon nanotubes. In the following calculations, we will choose a symmetric

hybrid system in the tunneling rates, $\Gamma_S = \Gamma_N = 0.1\Delta$, as an example, and also a strongly asymmetric system with $\Gamma_S = 10\Gamma_N$ as well for comparison with the results of experimental measurements.

A. Self energy and Andreev reflection spectrum

At first, we examine the dependence of the tunneling-induced electronic self-energy, Eq. (27), on the bias voltage and the temperature due to EPI under DTA. In Fig. 1, we plot the imaginary part of the first diagonal element of the vibrational dressed retarded self-energy, $\Sigma_{c11}^r(\omega)$, for the symmetric system with $g = 0$ (a) and $g = 1$ (b-d) at different bias voltages and temperatures. Without EPI, this quantity shows an obvious discontinuous at $\omega = \pm\Delta$ due to SC gap, and no voltage and temperature dependence [see Eqs. (8a) and (8e)]. In the presence of EPI, we find from Fig. 1(b) that it not only has the SC gap at $\omega = \pm\Delta$, but also develops vibronic replicas of the SC gap edges separated by integer multiples of phonon frequency ω_0 at the regions of $|\omega| > \Delta$ at low temperature; meanwhile at the subgap region, $|\omega| < \Delta$, it exhibits explicit stepwise structures whose widths are $2\omega_0$ or ω_0 , and heights are controlled by the Franck-Condon (FC) factors. These peaks and steps are all related to the opening of the inelastic transport channels, i.e. phonon assisted normal tunneling and/or Andreev reflection. Applying bias voltage just moves the steps in the subgap region towards the positive direction of frequency. At the corresponding points of peaks and steps, the real part of the self-energy shows peaks with singularities due to Kramers-Kronig relations (not shown here). Increasing temperature has two effects, smoothing the stepwise structures and developing additional SC edges within the subgap region.

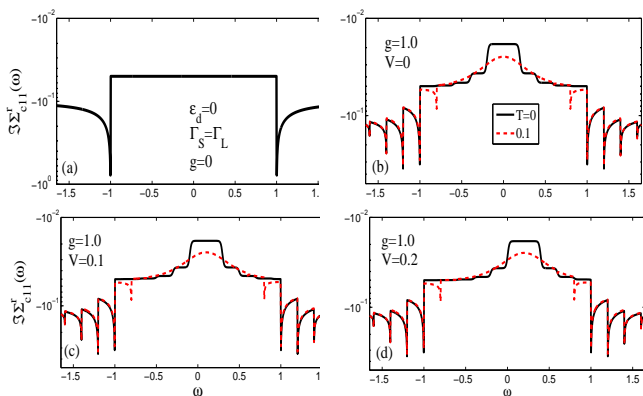


Figure 1: (Colour online) The imaginary part of the first diagonal element of the vibrational dressed retarded self-energy, $\Sigma_{c11}^r(\omega)$, are plotted for different bias-voltages, $V = 0$ (b), 0.1 (c), and 0.2 (d), respectively, at different temperatures, $T = 0$ and 0.1 . The parameters used for calculation are taken as: $\Gamma_N = \Gamma_S = 0.1$, $g = 1.0$. For comparison, the corresponding result for the system without EPI is plotted in (a).

Figure 2 shows the nondiagonal element of the vibrational dressed retarded self-energy, $\Sigma_{c12}^r(\omega)$, at $V = 0$. Its real part is found to be nonzero at the subgap region for the noninteracting system, which is ascribed to the SC proximity effect. According to Eq. (8e), it is equal to $\frac{1}{2} \frac{\Gamma_S \Delta}{\sqrt{\Delta^2 - \omega^2}}$, while its imaginary part is equal to 0. In the presence of EPI, the real part at the subgap region is suppressed due to the FC blockade.

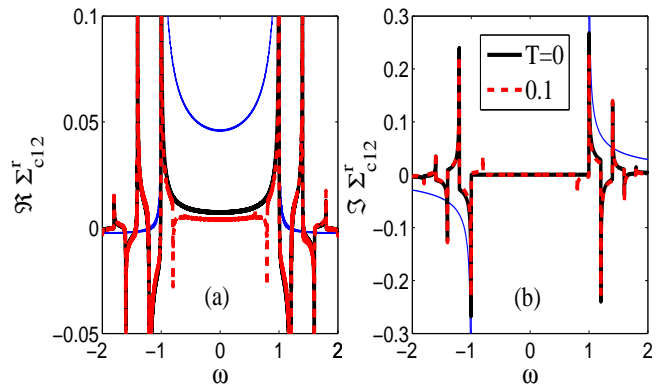


Figure 2: (Colour online) The real (a) and imaginary (b) parts of the nondiagonal element of the vibrational dressed retarded self-energy, $\Sigma_{c12}^r(\omega)$, at $V = 0$ and different temperatures, $T = 0$ and 0.1 . The other parameters are the same as those in Fig. 1. The thin-blue lines denote results for the system with $g = 0$.

We now analyze the Andreev reflection spectrum $T_A(\omega)$, since it is an underlying quantity to describe the nonequilibrium transport through the hybrid system in the subgap regime. We will compare the DTA results for $T_A(\omega)$, Eq. (30), with those from other approximations. The Andreev reflection spectrum of the SPA can be obtained by simply replacing the dressed self energies Eq. (27) with the bare ones, Eqs. (8a) and (8e), in calculating the pure electronic retarded GF $G_{c12}^r(\omega)$ in the formula Eq. (30) of Andreev reflection probability. In addition to SPA and DTA, another approximation namely as the polaron tunneling approximation is usually utilized to investigate the phonon assisted nonequilibrium transport through a normal-QD system perturbatively in strong coupling regime in literature.²⁰ The underlying physical essence of PTA is based on the atomic limit, within which the dot GF can be write down as the isolated QD after Lang-Firsov transformation and then use Dyson equation to couple the electrodes. It is nevertheless believed to be overestimated the electronic spectral density at high frequencies and predicts appearances of phonon side peaks in the conductance with varying energy level of QD in linear transport regime, which is inconsistent with previous experiment measurements.^{1,4} It is reported that the two drawbacks can be cured by the more rigorous DTA method.^{21,22}

Very recently, the PTA has been extended to study phonon assisted Andreev tunneling in the hybrid N-QD-S system, in which the bare retarded GF of the QD has

the form³¹

$$g_{11}^r(\omega) = \sum_{n=-\infty}^{\infty} \frac{w_n(1-n_0) + w_{-n}n_0}{\omega - (\varepsilon_d + n\omega_0) + i0^+}, \quad (34a)$$

$$g_{22}^r(\omega) = \sum_{n=-\infty}^{\infty} \frac{w_n(1-n_0) + w_{-n}n_0}{\omega + (\varepsilon_d + n\omega_0) + i0^+}, \quad (34b)$$

where n_0 represents the average occupation number on the QD, and $g_{12}^r(\omega) = g_{21}^r(\omega) = 0$. The electron GF can be evaluated by the Dyson equation, $G_c = g + g(\Sigma_N^r + \Sigma_S^r)G_c$. Substituting the calculated G_c into Eq. (30), we can evaluate the Andreev reflection probability $T_A(\omega)$ under PTA. Therefore, we show in Fig. 3 the comparison results of the DTA for $T_A(\omega)$ with those from SPA and PTA for the symmetric systems with $\varepsilon_d = 0, 0.1$, and -0.2 , respectively, in equilibrium case and at zero temperature.

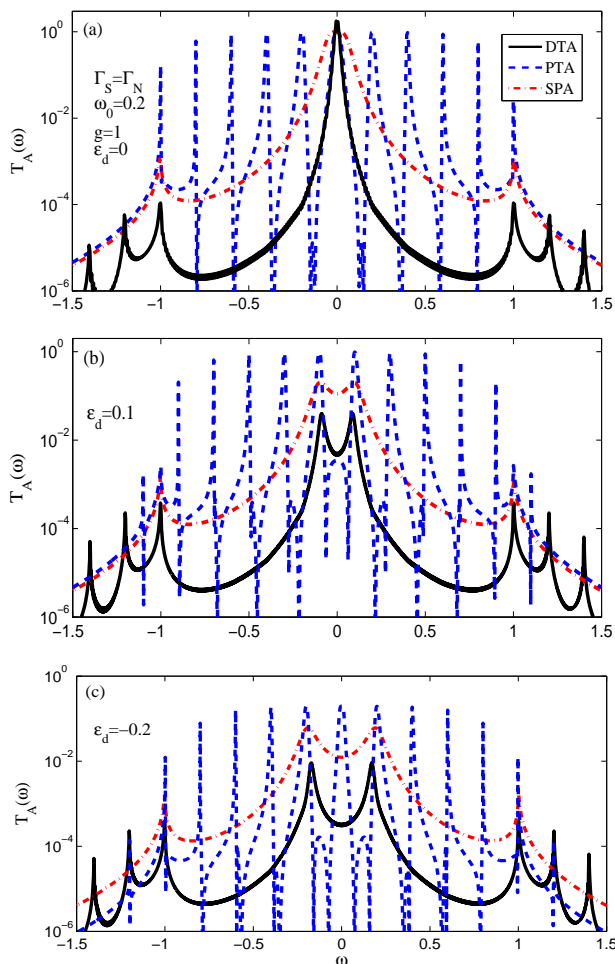


Figure 3: (Colour online) The Andreev reflection spectrum for the symmetric N-QD-S system $\Gamma_S = \Gamma_N$ with (a) $\varepsilon_d = 0$, (b) 0.1 , and (c) -0.2 at zero bias voltage and zero temperature. The calculated results correspond to the different approximations: DTA (solid-black line), PTA (dashed-blue line), and SPA (dashed-dotted-red line).

One can find from Fig. 3 that the main feature of the

DTA results is remarkably narrowing of the Andreev resonance in comparison with those of SPA, both of which show no phonon-assisted side peaks in the subgap region $|\omega| < \Delta$; On the contrary, the PTA results exhibit obvious subgap phonon side peaks at $\omega = \pm(\varepsilon_d + n\omega_0)$ ($n \geq 0$) with nearly equal height.

For the electron-hole symmetric case $\varepsilon_d = \mu_S = 0$, the Andreev reflection reaches resonance when the energy of incident electron is aligned with the Fermi energy of the SC electrode, i.e. $\omega = 0$. Moreover, this central resonant peak exhibits remarkably rapid decrease for both DTA and PTA results, if the incident electron moves away from the resonant point.

In this QD system, the dot energy level can be tuned by applying gate voltage. When the dot level ε_d is tuned away from the symmetric point $\mu_S = 0$, there are two Andreev resonant peaks located at $\omega = \pm|\varepsilon_d|$ for the SPA and DTA results, as the case of noninteracting system, but with a reduced amplitude. The situation may however be quite different for the PTA results. For the case of $\varepsilon_d = \pm 0.2$ (only the result of $\varepsilon_d = -0.2$ is plotted in Fig. 3(c)), the zero energy resonant peak is still remaining due to phonon assisted process, which is responsible for the appearance of the phonon side peak at the Andreev linear conductance by PTA as shown in Fig. 6 below.

Once again it should be emphasized that the PTA does not take into account vibronic dressing effect on electronic tunneling, while the more rigorous DTA indeed does, leading to complex dependence of the tunneling self-energies on bias voltage and temperature. That is the reason that the two methods predict great different Andreev reflection spectrum, which determines different exotic transport properties of the hybrid QD system at the subgap region, as we will see below.

Moreover, we examine the bias voltage dependence of the Andreev reflection by DTA. As shown in Fig. 4, the resonant peak is slightly suppressed with increasing bias voltage, which can be ascribed to bias voltage dependent retarded self-energy. It is this suppression that results in a surprise decrease of the elastic tunneling current with increase of bias voltage.

Notice that the present theoretical method, DTA, can properly describe the dynamic properties of the EPI system not only in the strong coupling regime but also in the relatively weak coupling regime.²² At last of this section, we therefore analyze the Andreev reflection spectrum by DTA for the strongly asymmetric system with $\Gamma_S = 10\Gamma_N$ and different EPI constants, $g = 0.5, 0.75$, and 1.0 . In Fig. 5, we show the DTA results for the Andreev reflection spectrum at these cases with $\varepsilon_d = 0$ and 0.05 . The thin lines in this figure denote the corresponding results for the system without EPI. It is clear that owing to the strong SC proximity effect and weak coupling to the normal lead, two nearly resonant ingap states, i.e. the Andreev bound states, are distinctly emerging and cause subgap peaks in the Andreev reflection spectrum centered at energies $\pm\sqrt{\varepsilon_d^2 + \Gamma_S^2}/4$. The EPI effect is two

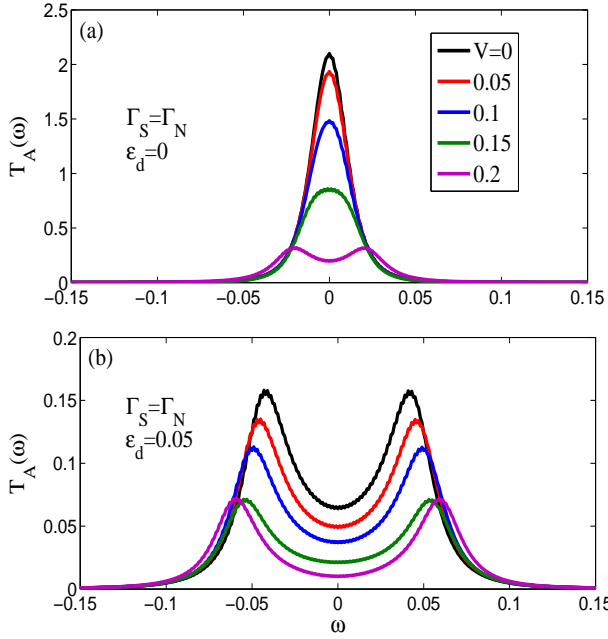


Figure 4: (Colour online) The bias voltage dependence of the Andreev reflection spectrum in the DTA for the symmetric systems with $\epsilon_d = 0$ and 0.05 at zero temperature.

folds. For the electron-hole symmetric system $\epsilon_d = 0$, inelastic scattering results in the resonant peaks shrinking progressively and becoming nearly single resonant peak with enhanced height at $\omega = 0$ as EPI constant increases; while for the system $\epsilon_d = 0.05$, the resonant peaks are also gradually shrinking but eventually pinning at $\pm\epsilon_d$ and a suppressed Andreev reflection spectrum at $\omega = 0$.

B. Linear Andreev conductance

The DTA result for the linear Andreev conductance G can be easily calculated from Eq. (31). At zero temperature, we have

$$G = \left. \frac{dI_A}{dV} \right|_{V=0} = \frac{4e^2}{h} w_0^2 |T_A(0)|^2 = \frac{4e^2}{h} \left\{ \frac{w_0 \Gamma_N \Re \Sigma_{c12}^r(0)}{\epsilon_d^2 + [\Im \Sigma_{c11}^r(0)]^2 + [\Re \Sigma_{c12}^r(0)]^2} \right\}^2, \quad (35)$$

since $\Re \Sigma_{c11(22)}^r(0) = \Im \Sigma_{c12}^r(0) = 0$, and $\Im \Sigma_{c11(22)}^r(0) = -iw_0 \Gamma_N / 2$. While the PTA result for conductance can be simply obtained from Eq. (16) as $G_{\text{PTA}} = \frac{4e^2}{h} |T_A(0)|^2$ in the place of the Andreev reflection probability with the PTA one. We plot the two results as functions of dot level at different temperatures for the symmetric system in Fig. 6.

For comparison, the Andreev conductance for noninteracting system is also plotted in Fig. 6, which shows the following features: (1) the maximum value $G_0 = 4e^2/h$ for the resonant system $\epsilon_d = 0$ at zero temperature; (2)

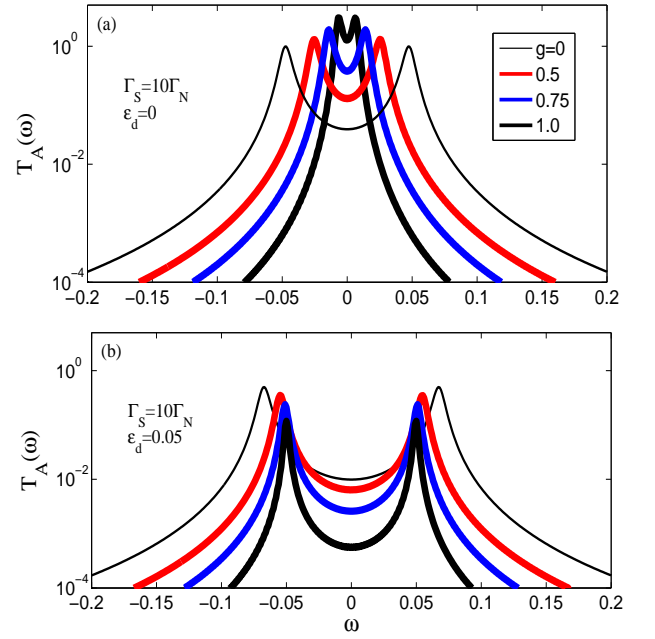


Figure 5: (Colour online) The Andreev reflection spectrum in the DTA at zero bias voltage and zero temperature for the asymmetric N-QD-S system with $\Gamma_S = 10\Gamma_N$, and different values of the EPI constant, $g = 0, 0.5, 0.75$, and 1.0 . (a) is for the QD with the level $\epsilon_d = 0$, and (b) is for $\epsilon_d = 0.05$.

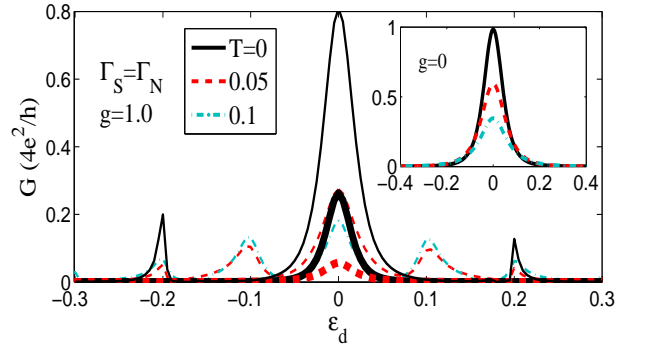


Figure 6: (Colour online) The linear Andreev conductance G for the symmetric system as a function of the resonant level ϵ_d of the QD with $g = 1$ at different temperatures $T = 0, 0.05$, and 0.1 . The thick lines correspond to the DTA results, while the thin lines to the PTA results. Inset: the corresponding results for the system in absence of EPI.

with increasing temperature, it is suppressed, but does not exhibit thermal broadening as the normal conductance does. For the EPI system, we observe a similar temperature behavior for the DTA results. Besides, the DTA predicts remarkable suppression of the Andreev conductance, $G = 0.22G_0$, even for the resonant system $\epsilon_d = 0$ at zero temperature, which is ascribed to the large suppression of the nondiagonal element of the self-energy at the subgap region [see Fig. 2(a)] and an extra w_0^2 factor in Eq. (35) due to the FC blockade.

More importantly, we find that the linear Andreev con-

ductance G exhibits no phonon side peaks as a function of the gate voltage, when ε_d crosses the vibronic frequency. In specific, Eq. (35) shows that G is proportional to ε_d^{-4} , indicating that the effect of the strong EPI is just to remarkably narrow the width of its resonance peak as the gate voltage is swept. This result is completely conflict with the PTA calculations, as indicated by the thin lines in Fig. 6. For instance, the PTA calculations predicts two kinds of phonon assisted peaks: one is located at the phonon frequency, $|\varepsilon_d| = \omega_0 = 0.2$, at zero temperature; the other one emerges at half of the phonon frequency, $|\varepsilon_d| = \omega_0/2 = 0.1$, with increasing temperatures. From mathematic point of view, the former one is stemming from the zero energy resonance in the Andreev reflection spectrum. While the later one results from the phonon assisted resonances of the Andreev reflection near $\omega = 0$ at $\omega = \pm\omega_0/2 = \pm 0.1$, as shown in Fig. 3(b), since these nearby peaks will make non-negligible contribution to integrals over energy in calculating linear-response conductance at sufficiently high temperature. It is noticed that albeit two peaks are also predicted at $\omega = \pm 0.1$ for the Andreev reflection spectrum by DTA, their heights are only two orders lower than those of PTA. They are therefore too weak to induce phonon side peak in linear transport.

Furthermore, we should notice that, as in the normal QD system, these appearance of phonon side peaks in linear response conductance is just an artifact of the used approximative method and is in fact unphysical. Since at zero bias voltage, the incident electron has at almost the same energy with the emitting electron, energy conservation does not allow the vibration to be excited during tunneling process. As in the normal QD system, the DTA corrects this artifact of the PTA by more precisely taking account of the vibrational effect on electronic tunneling self-energy.

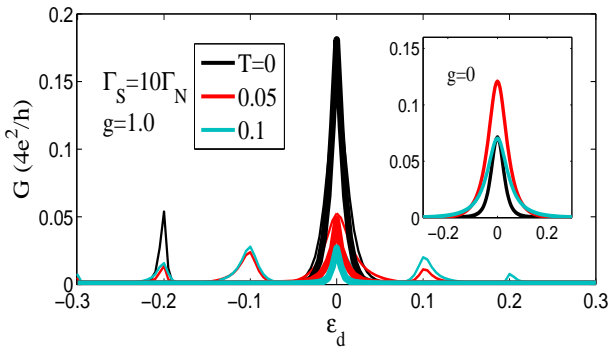


Figure 7: (Colour online) The linear Andreev conductance G for the asymmetric system $\Gamma_S = 10\Gamma_N$. Other parameters are the same as those in Fig. 6

Finally in this subsection, we investigate the Andreev conductance for the asymmetric system $\Gamma_S = 10\Gamma_N$. In the same way, no phonon side peak is found for the DTA calculations as shown in Fig. 7. At this case, the noninteracting system exhibits opposite temperature behavior

to the symmetric system. The EPI effect abnormally enhances the central peak of the zero-temperature conductance due to the shrinking behavior at $\varepsilon_d = 0$ in Fig. 5(a). As moving away from the electron-hole symmetric point, the EPI effect causes more rapidly narrowing of the peak of the conductance because of big suppression of the Andreev reflection spectrum at $\omega = 0$ in Fig. 5(b).

C. Andreev Current and differential conductance

We now study the nonlinear transport at the sub-gap region. In Figs. 8 and 9, we plot the Andreev currents I_A and corresponding differential conductances $g_A = dI_A/dV$ as functions of bias voltage $V > 0$ for the symmetric systems with $\varepsilon_d = 0$ and 0.05, respectively, at zero temperature. It would be very useful for understanding the calculated results by analyzing the respective contributions of the elastic and inelastic Andreev processes. We therefore plot their corresponding elastic and inelastic contributions, and the total results as well.

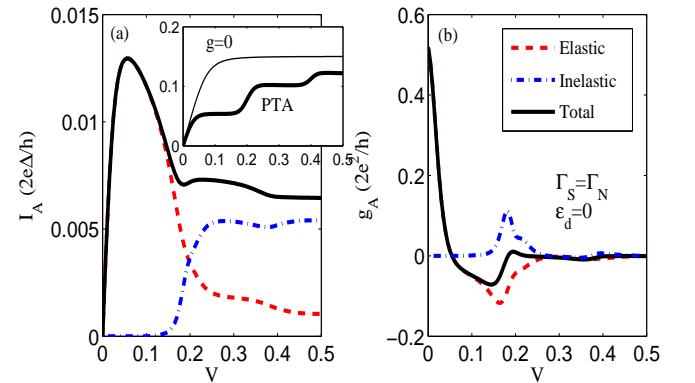


Figure 8: (Colour online) (a) The calculated total current (solid line), elastic current (dashed line), inelastic current (dotted-dashed line); and (b) the corresponding differential conductances as functions of bias voltage for a symmetric system with $\varepsilon_d = 0$ at zero temperature. The inset shows the PTA result (thick line) for the Andreev current and the current for noninteracting system (thin line).

At zero temperature, the elastic current formula Eq. (33) can be simplified as

$$I_{el} = \frac{2e}{h} w_0^2 \int_{-V}^V d\omega T_A(\omega). \quad (36)$$

The elastic current rises monotonously as usual at the beginning, and then suffers a decrease with increase of the bias voltage. Differentiating Eq. (36) with respect to V , the elastic differential conductance can be written as two parts $g^{el} = dI_{el}/dV = g_1^{el} + g_2^{el}$, with

$$g_1^{el} = \frac{4e^2}{h} w_0^2 T_A(V), \quad (37)$$

and

$$g_2^{el} = \frac{2e^2}{h} w_0^2 \int_{-V}^V d\omega \frac{\partial T_A(\omega)}{\partial V}. \quad (38)$$

The first term, g_1^{el} , is proportional to the Andreev reflection $T_A(V)$ and results in a zero-bias maximum for the electron-hole symmetric system, and a nonzero-bias maximum, i.e. a resonant peak at $V = \varepsilon_d$, for the system with $\varepsilon_d = 0.05$ due to peak splitting of the Andreev reflection spectrum as shown in Fig. 4(b); while the second term, g_2^{el} , is stemming from the bias voltage dependent Andreev reflection and makes negative contribution, which is responsible for decrease of the elastic current.

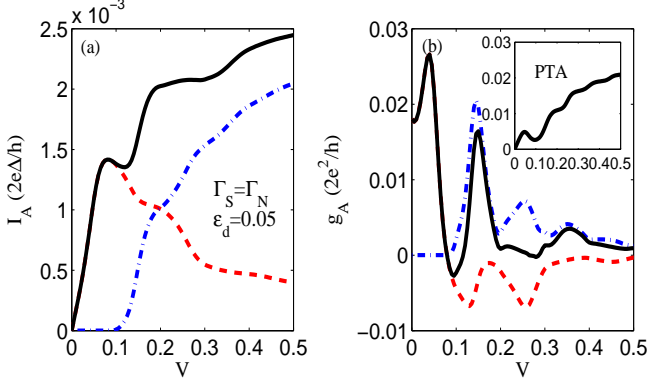


Figure 9: (Colour online) The same figure as Fig. 8 but for the system with $\varepsilon_d = 0.05$.

The inelastic current has a threshold at the onset for inelastic Andreev reflection processes, $V = \omega_0 = 0.2$, for the electron-hole symmetric system $\varepsilon_d = 0$, for phonon emission which shows up as an abrupt increase of the inelastic current and a peak in the differential conductance as shown in Fig. 8. This observation can be interpreted, from mathematic point of view, by the dominant terms of the zero-temperature inelastic current

$$I_{in} \simeq \frac{4e}{h} w_0 w_1 \left(\int_{\omega_0 - V}^V + \int_{-V}^{V - \omega_0} \right) d\omega T_A(\omega) + \frac{2e}{h} w_1^2 \int_{\omega_0 - V}^{V - \omega_0} d\omega T_A(\omega). \quad (39)$$

From physical perspective, such inelastic process can be illustrated in Fig. 10(a): an electron with energy ω_0 in the left normal lead can first emit a phonon to tunnel into the dot, and then enter the right SC lead to form a Cooper pair by picking up an electron originally in the dot, and finally reflect a hole back into the left lead.

More interestingly, as we consider the system moving away from the electron-hole symmetric case, i.e. $\varepsilon_d \neq 0$, we find a novel inelastic transport channel which is opening even at a bias voltage lower than the phonon energy. To be specific, Fig. 9(b) exhibits a relatively sharp peak at $V = 0.15 < \omega_0$ in the inelastic differential conductance for the system with $\varepsilon_d = 0.05$. This peak can be ascribed

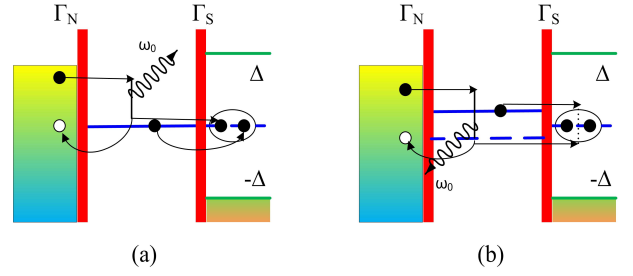


Figure 10: (Colour online) Schematic diagram of the phonon emission assisted Andreev reflection processes involved in Figs. 8 and 9, respectively. Solid (open) circles denote the states of quasiparticles (quasiholes), and the arrows stand for directions of their tunneling. See text for more detail.

to a new sort of phonon assisted Andreev reflection process as described in Fig. 10(b): if the dot level is aligned at a positive energy, an electron with energy $\omega_0 - \varepsilon_d$ in the left lead can first transverse the dot at the opposite energy level $-\varepsilon_d$ by emitting a phonon, and pick up an electron in the dot at the level ε_d to form a Cooper pair. In this spirit, this sort of phonon assisted Andreev reflection can emerge at the condition $V = -|\varepsilon_d| + n\omega_0$ ($n > 0$). It is different from a N-QD-N system, where phonon assisted resonant tunneling will occur when the symmetrically applied bias voltage obeys the condition $V = 2(|\varepsilon_d| + n\omega_0)$. Therefore, this newly predicted intriguing peak can be considered as a distinctive signature of the phonon assisted Andreev tunneling process. From Fig. 9(b), another peak in the inelastic current is found at $V = 0.25$, which is stemming from the remaining effect of the peak splitting (its vibratic replica) in the Andreev reflection spectral function as shown in Fig. 4(b).

It is noticed that not only the inelastic Andreev current but also its elastic component exhibits phonon assisted features stated above since the opening of new inelastic processes will inevitably change the retarded self-energy. For instance, when the inelastic current channel is active, the term g_2^{el} becomes predominant over the first term g_1^{el} , leading to further decrease of the elastic current and peaks (with negative values) of the elastic differential conductance. For the electron-hole symmetric system, $\varepsilon_d = 0$, this behavior causes a negative differential conductance (NDC), which was observed in a recent experimental measurement.²⁸ However, the PTA result predicts completely different I - V characteristics, no appearance of NDC, for the symmetric system. For the electron-hole asymmetric system, $\varepsilon_d = 0.05$, on the contrary, it is observed that the relatively strong inelastic peaks compensate the decrease of the elastic current and lead to nearly disappearance of NDC by DTA results. Nevertheless, the PTA calculation still exhibits an unambiguous NDC in the inset of Fig. 9(b).

The I - V characteristics of the asymmetric system $\Gamma_s = 10\Gamma_N$ is shown in Fig. 11 for the case of $\varepsilon_d = 0$ and $g = 0.5$. The subgap differential conductance g_A shows a nonzero-bias maximum. This nonzero-bias anomaly has

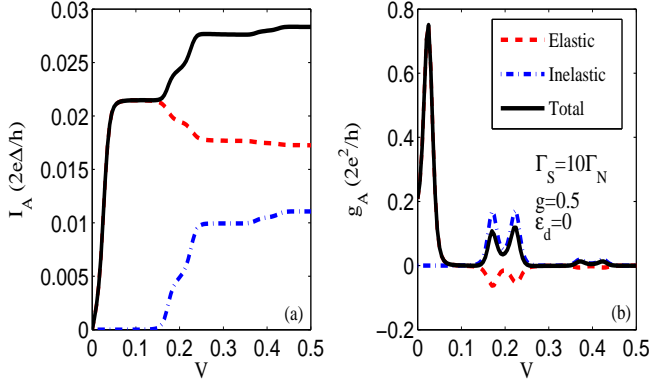


Figure 11: (Colour online) The same figure as Fig. 8 but for the asymmetric system with $\Gamma_S = 10\Gamma_N$ and a weak EPI constant $g = 0.5$.

different origin from that of the symmetric system with $\varepsilon_d \neq 0$, which is stemming from the peak splitting of the Andreev reflection spectrum because of nonzero energy of the localized dot state. Here, the anomaly is due to distinct emergence of the ingap bound state, the Andreev state, in the extremely asymmetric tunnel-coupling. This bound state also induces peak splitting of the Andreev reflection spectrum as demonstrated in Fig. 5(a) as long as the EPI is not considerably strong. In addition, this peak splitting also affects the inelastic current, leading to a double-peak in the g_A - V curve near the point $V = \omega_0 = 0.2$ where the inelastic channel is just opening.

D. Zero-frequency shot noise

In what follows, we analyze the zero-frequency shot noise at zero temperature, which can be calculated using a simplified expression according to the Eq. (32)

$$S_A = 2eI_A - \frac{4e^2}{h}\Gamma_N^2 \sum_{nmn'm'} w_n w_m w_{n'} w_{m'} \times \int_{\omega_1}^{\omega_2} d\omega T_A^2(\omega), \quad (40)$$

with $\omega_1 = \max(n\omega_0 - V, n'\omega_0 - V)$ and $\omega_2 = \min(V - m\omega_0, V - m'\omega_0)$. We can also separate the shot noise as two contributions of elastic and inelastic parts, $S_A = S_{el} + S_{in}$, as

$$S_{el} = 2eI_{el} - \frac{4e^2}{h}\Gamma_N^2 w_0^4 \int_{-V}^V d\omega T_A^2(\omega), \quad (41a)$$

$$S_{in} = 2eI_{in} - \frac{4e^2}{h}\Gamma_N^2 w_0^2 (2w_0 + w_1) w_1 \times \left(\int_{\omega_0 - V}^V + \int_{-V}^{V - \omega_0} \right) d\omega T_A^2(\omega) - \frac{16e^2}{h}\Gamma_N^2 w_0^2 w_1^2 \int_{\omega_0 - V}^{V - \omega_0} d\omega T_A^2(\omega). \quad (41b)$$

In Fig. 12(a), we plot the calculated shot noise, its two parts (normalized by $4e^2\Delta/h$), and the total current (normalized by $2e\Delta/h$) as functions of bias voltage $V > 0$ for the symmetric system with $\varepsilon_d = 0$ and $g = 0.75$. It is observed that for the QD $\varepsilon_d = 0$, the elastic and inelastic noises inherit the same overall profiles as their corresponding currents with increasing bias voltage. We also show the Fano factors, defined as $F = S_A/e^*I_A$ (since the Andreev reflection corresponds to transferring twice the electron charge $e^* = 2e$), in Fig. 12(b) for three values of the EPI parameters, $g = 0.5, 0.75$, and 1 . We find that the noise is greatly enhanced with increasing EPI strength. The Fano factor nearly approaches the value 1 for the case of $g = 1$ at high bias voltage region, while $F \approx 0.25$ for the noninteracting N-QD-S system. We can interpret the EPI-induced enhancement of noise as follows. The zero-temperature noise for the noninteracting system is simplified from Eq. (15) as

$$S_A = 2eI_A - \frac{4e^2}{h}\Gamma_N^2 \int_{-V}^V d\omega T_A^2(\omega). \quad (42)$$

Because of the second term, the Fano factor is quite small. With increasing EPI strength, the contribution of the second term (and the third term) becomes more and more weaker due to the FC factors w_0 and w_1 in Eq. (41a) and (41b) (FC blockade effect), for instance, $w_0 = w_1 = 0.368$ at $g = 1$. It is the FC blockade that induces enhancement of shot noise.

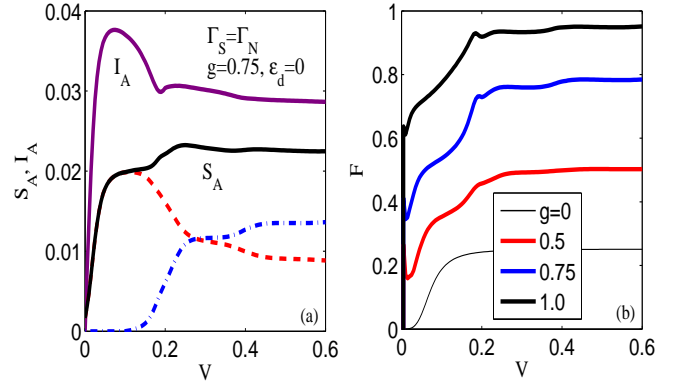


Figure 12: (Colour online) (a) The zero-temperature shot noise (solid black line), and its elastic (dashed red line) and inelastic (dotted-dashed blue line) parts (normalized by $4e^2\Delta/h$) as functions of bias voltage for a symmetric N-QD-S with $\varepsilon_d = 0$ and $g = 0.75$. The total Andreev current is also plotted as a solid purple line; (b) The Fano factors for the system $\varepsilon_d = 0$ with different EPI constants $g = 1.0$ (black line), 0.75 (blue line), and 0.5 (red line). For comparison, the thin line denotes the Fano factor of the system without EPI.

For the asymmetric tunnel-coupling case considered in the present paper, $\Gamma_N = 10\Gamma_S$, the situation is quite different as illustrated in Fig. 13. First of all, the noninteracting system has a greater Fano factor, $F \approx 0.5$, than that of the symmetric system since the second term in Eq. (42) has a smaller contribution due to the peak split-

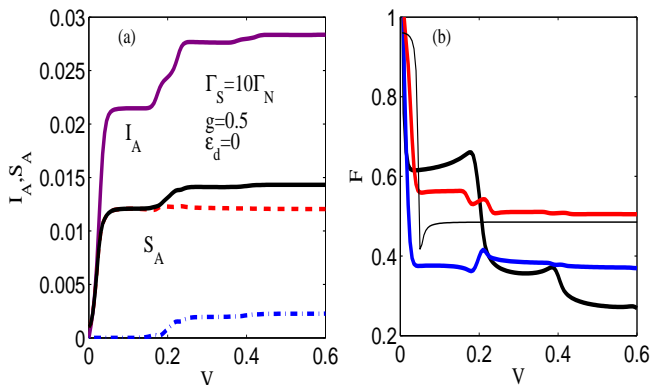


Figure 13: (Colour online) This figure is the same as Fig. 12 except for the asymmetric system with $\Gamma_S = 10\Gamma_N$, and $g = 0.5$ in (a).

ting in the Andreev reflection spectrum with suppressed magnitude as demonstrated in Fig. 5(a). However, the splitting peaks will become shrinking and enhanced with increasing EPI strength, even become probably a single resonant peak at the case of $g = 1$. As a result, the contribution of the second and third terms in Eqs. (41a) and (41b) becomes gradually more and more important with increasing EPI strength, in spite of the FC factor. Consequently, strong EPI could lead to suppression of shot noise at large bias voltage region, where the inelastic channel is opening. For instance, $F \approx 0.27$ at $V = 0.6$ for the system with $g = 1$ in Fig. 13(b). While if the inelastic channel is not opening at small bias voltage region ($V \leq 0.2$ for the present case), only the second term in Eq. (41a) is necessary to be considered. This fact will therefore result in an enhancement of noise for the case of $g = 1$ due to FC blockade effect $w_0 = 0.368$, but still a suppression for the case of $g = 0.75$ due to a bigger $w_0 = 0.57$.

IV. CONCLUSION

In conclusion, we have present a theory of the FCS of vibrational assisted electronic tunneling through a hybrid N-QD-S system in the subgap region on the basis of the Lang-Firsov canonical transformation for the local EPI and NGF method. In order to examine the interplay between the vibrational modified tunneling and the SC proximity effect, we have generalized the DTA decoupling scheme, which has been recently developed to study vibrational assisted stationary and transient tunneling in the N-QD-N system, to the hybrid system. Since this method takes more rigorous account of the phononic propagator in evaluation of the electronic GF, it is believed to provide correct description for phonon assisted electronic tunneling in the polaronic regime and even the crossover regime, $g^2\omega_0 \leq \Gamma_N$, by comparison with other methods, for example, the SPA and the PTA. Besides, the DTA can provide an explicit analytical formula for

the cumulant generating function for the vibrational assisted Andreev tunneling, and give analytical expressions for the current, zero-frequency shot noise, and etc.

In the first step we have discussed in detail phonon effects on the Andreev reflection spectrum for the symmetric and asymmetric hybrid systems and their bias voltage dependence, since it is the underlying sole physical quantity to characterize subgap transport properties of a hybrid N-QD-S system. Different from the PTA results for the subgap Andreev reflection spectrum, the DTA results have predicted no appearance of phonon assisted side peaks, instead a remarkably narrowed single peak and/or splitting peak in the subgap region.

In the second step we have investigated inelastic effects on the subgap I - V characteristics. The PTA calculations predict that the linear Andreev conductance G will show phonon assisted side peaks as the gate voltage is swept. Noticeably, one of the most important results in the present studies is to correct the unphysical result and predict a single narrowed peak in the G - ε_d curves. Another intriguing result is about inelastic effects on the nonlinear transport. Two kinds of phonon assisted Andreev reflection processes are identified for the electron-hole symmetric system $\varepsilon_d = 0$ and the asymmetric system $\varepsilon_d \neq 0$, respectively. In particular, a novel upward step in current is found for the latter case, showing a resonant peak in its differential conductance g - V curve, when the inelastic Andreev reflection channel is opening at $V = -|\varepsilon_d| + \omega_0$. It is noticed that this phonon assisted resonant tunneling condition, $V < \omega_0$, is quite different from that of normal electronic tunneling at N-QD-N system. It is therefore can be regarded as a representative signature of the vibronic assisted Andreev reflection. Moreover, for the former case a pronounced decrease of the elastic part of the current is observed with increasing bias voltage, leading to a NDC at small bias voltage region. We have pointed out that this NDC is stemming from the bias-voltage induced suppression of the Andreev reflection spectrum.

In the final step we have examined the zero-frequency shot noise at zero temperature. By analyzing the Fano factor, we have displayed that vibronic effect could induce either enhancement of noise in the electron-hole symmetric case or suppression of noise in the electron-hole asymmetric case at large bias voltage limit.

Some of these predictions, for instant, no appearance of phonon assisted side peak in the linear conductance and a NDC behavior in the nonlinear current at the subgap region, are in good qualitative agreement with recent experimental measurement on inelastic Andreev tunneling on a Carbon nanotube QD. We hope that our other findings could be tested in the future experiments.

Acknowledgments

This work was supported by Projects of the National Basic Research Program of China (973 Program) un-

der Grant No. 2011CB925603, and the National Science Foundation of China, Specialized Research Fund for

the Doctoral Program of Higher Education (SRFDP) of China.

- ¹ H. Park, J. Park, A. Lim, E. Anderson, A. Allvisatos, and P. McEuen, *Nature (London)* **407**, 57 (2000).
- ² J. Park, A.N. Pasupathy, J.I. Goldsmith, C. Chang, Y. Yaish, J.R. Petta, M. Rinkoski, J.P. Sethna, H. Abruna, P.L. McEuen, and D.C. Ralph, *Nature* **417**, 722 (2002); N.B. Zhitenev, H. Meng, and Z. Bao, *Phys. Rev. Lett.* **88**, 226801 (2002).
- ³ E.M. Weig, R.H. Blick, T. Brandes, J. Kirschbaum, W. Wegscheider, M. Bichler, and J.P. Kotthaus, *Phys. Rev. Lett.* **92**, 046804 (2004); L.H. Yu, Z.K. Keane, J.W. Ciszek, L. Cheng, M.P. Stewart, J.M. Tour, and D. Natelson, *Phys. Rev. Lett.* **93**, 266802 (2004); L.H. Yu and D. Natelson, *Nano Lett.* **4**, 79 (2004); A.N. Pasupathy, J. Park, C. Chang, A.V. Soldatov, S. Lebedkin, R.C. Bialczak, J.E. Grose, L.A.K. Donev, J.P. Sethna, D.C. Ralph, and P.L. McEuen, *Nano Lett.* **5**, 203 (2005).
- ⁴ B.J. LeRoy, S.G. Lemay, J. Kong, and C. Dekker, *Nature* **432**, 371 (2004); B.J. LeRoy, J. Kong, V.K. Pahilwani, C. Dekker, and S.G. Lemay, *Phys. Rev. B* **72**, 075413 (2005); S. Sapmaz, P. Jarillo-Herrero, Ya.M. Blanter, C. Dekker, and H.S.J. van der Zant, *Phys. Rev. Lett.* **96**, 026801 (2006).
- ⁵ A. Mitra, I. Aleiner, and A.J. Millis, *Phys. Rev. B* **69**, 245302 (2004); *Phys. Rev. Lett.* **94**, 076404 (2005).
- ⁶ J. Koch and F. von Oppen, *Phys. Rev. Lett.* **94**, 206804 (2005); J. Koch and F. von Oppen, *Phys. Rev. B* **72**, 113308 (2005); J. Koch, M.E. Raikh, and F. von Oppen, *Phys. Rev. Lett.* **95**, 056801 (2005).
- ⁷ A. Zazunov, D. Feinberg, and T. Martin, *Phys. Rev. B* **73**, 115405 (2006).
- ⁸ X.Y. Shen, B. Dong, X.L. Lei, and N.J.M. Horing, *Phys. Rev. B* **76**, 115308 (2007); B. Dong, X.L. Lei, and N.J.M. Horing, *IEEE Sensor Journal* **8**, 885 (2008); B. Dong, H.Y. Fan, X.L. Lei, and N.J.M. Horing, *J. Appl. Phys.* **105**, 113702 (2009).
- ⁹ T. Frederiksen, M. Brandbyge, N. Lorente, and A.P. Jauho, *Phys. Rev. Lett.* **93**, 256601 (2004); M. Paulsson, T. Frederiksen, and M. Brandbyge, *Phys. Rev. B* **72**, 201101 (2005); T. Frederiksen, M. Paulsson, M. Brandbyge, and A.P. Jauho, *Phys. Rev. B* **75**, 205413 (2007).
- ¹⁰ L. de la Vega, A. Martín-Rodero, N. Agraït, and A. Levy Yeyati, *Phys. Rev. B* **73**, 075428 (2006).
- ¹¹ J.K. Viljas, J.C. Cuevas, F. Pauly, and M. Häfner, *Phys. Rev. B* **72**, 245415 (2005); R. Egger and A.O. Gogolin, *Phys. Rev. B* **77**, 113405 (2008).
- ¹² O. Entin-Wohlman, Y. Imry, and A. Aharony, *Phys. Rev. B* **80**, 035417 (2009).
- ¹³ K. Haule and J. Bonča, *Phys. Rev. B* **59**, 13087 (1999); E.G. Emberly and G. Kirzenow, *Phys. Rev. B* **61**, 5740 (2000); B. Dong, H.L. Cui, and X.L. Lei, *Phys. Rev. B* **69**, 205315 (2004); B. Dong, H.L. Cui, X.L. Lei, and N.J.M. Horing, *Phys. Rev. B* **71**, 045331 (2005).
- ¹⁴ K. Flensberg, *Phys. Rev. B* **68**, 205323 (2003).
- ¹⁵ A. Martin-Rodero, A. Levy Yeyati, F. Flores, and R.C. Monreal, *Phys. Rev. B* **78**, 235112 (2008); R.C. Monreal and A. Martin-Rodero, *Phys. Rev. B* **79**, 115140 (2009); R.C. Monreal, F. Flores, and A. Martin-Rodero, *Phys. Rev. B* **82**, 235412 (2010).
- ¹⁶ M. Galperin, A. Nitzan, and M.A. Ratner, *Phys. Rev. B* **73**, 045314 (2006); M. Galperin, A. Nitzan, and M.A. Ratner, *Phys. Rev. B* **74**, 075326 (2006); R. Härtle, C. Benesch, and M. Thoss, *Phys. Rev. B* **77**, 205314 (2008); R. Härtle, M. Butzin, O. Rubio-Pons, and M. Thoss, *Phys. Rev. Lett.* **107**, 046802 (2011).
- ¹⁷ A. Zazunov and T. Martin, *Phys. Rev. B* **76**, 033417 (2007).
- ¹⁸ T.L. Schmidt, and A. Komnik, *Phys. Rev. B* **80**, 041307 (2009); R. Avriller and A. Levy Yeyati, *Phys. Rev. B* **80**, 041309 (2009); F. Haupt, T. Novotný, and W. Belzig, *Phys. Rev. Lett.* **103**, 136601 (2009); F. Haupt, T. Novotný, and W. Belzig, *Phys. Rev. B* **82**, 165441 (2010).
- ¹⁹ R. Avriller and T. Frederiksen, *Phys. Rev. B* **86**, 155411 (2012).
- ²⁰ S. Maier, T.L. Schmidt, and A. Komnik, *Phys. Rev. B* **83**, 085401 (2011).
- ²¹ B. Dong, G.H. Ding, and X.L. Lei, *Phys. Rev. B* **88**, 075414 (2013).
- ²² R. Seoane Souto, A.L. Yeyati, A. Martin-Rodero, and R.C. Monreal, *Phys. Rev. B* **89**, 085412 (2014).
- ²³ L. Hofstetter, A. Geresdi, M. Aagesen, J. Nygård, C. Schönenberger, and S. Csonka, *Phys. Rev. Lett.* **104**, 246804(2010).
- ²⁴ R. S. Deacon, Y. Tanaka, A. Oiwa, R. Sakano, K. Yoshida, K. Shibata, K. Hirakawa, and S. Tarucha, *Phys. Rev. Lett.* **104**, 076805 (2010); *Phys. Rev. B* **81**, 121308 (2010).
- ²⁵ K.J. Franke, G. Schulze, and J.J. Pascual, *Science* **332**, 940 (2011).
- ²⁶ J.-D. Pillet, C.H.L. Quay, P. Morfin, C. Bena, A. Levy Yeyati, and P. Joyez, *Nat. Phys.* **6**, 965 (2010); T. Dirks, T.L. Hughes, S. Lal, B. Uchoa, Y.-F. Chen, C. Chialvo, P.M. Goldbart, and N. Mason, *Nat. Phys.* **7**, 386 (2011); E.J.H. Lee, X. Jiang, M. Houzet, R. Aguado, C.M. Lieber, and S. De Franceschi, *Nat. Nanotechnol.* **9**, 79 (2013).
- ²⁷ L. Hofstetter, S. Csonka, J. Nygård, and C. Schönenberger, *Nature (London)* **461**, 960 (2009); L.G. Herrmann, F. Portier, P. Roche, A.L. Yeyati, T. Kontos, and C. Strunk, *Phys. Rev. Lett.* **104**, 026801 (2010); L. Hofstetter, S. Csonka, A. Baumgartner, G. Fülöp, S. d'Hollosy, J. Nygård, and C. Schönenberger, *Phys. Rev. Lett.* **107**, 136801 (2011); J. Schindele, A. Baumgartner, and C. Schönenberger, *Phys. Rev. Lett.* **109**, 157002 (2012).
- ²⁸ J. Gramich, A. Baumgartner, and C. Schönenberger, *Phys. Rev. Lett.* **115**, 216801 (2015).
- ²⁹ P. Zhang and Y.-X. Li, *J. Phys.: Condens. Matter* **21**, 095602 (2009).
- ³⁰ D. Golež, J. Bonča, and R. Žitko, *Phys. Rev. B* **86**, 085142 (2012).
- ³¹ S.N. Zhang, W. Pei, T.F. Fang, and Q.F. Sun, *Phys. Rev. B* **86**, 104513 (2012).
- ³² K. Bocian and W. Rudziński, *Eur. Phys. J. B* **88**, 50 (2015).
- ³³ J. Barański and T. Domański, *J. Phys.: Condens. Matter* **27**, 305302 (2015).
- ³⁴ P. Stadler, W. Belzig, and G. Rastelli, *Phys. Rev. Lett.*

- 117**, 197202 (2016).
- ³⁵ A. Komnik and A.O. Gogolin, Phys. Rev. Lett. **94**, 216601 (2005); A.O. Gogolin and A. Komnik, Phys. Rev. B **73**, 195301 (2006).
- ³⁶ G.D. Mahan, *Many-Particle Physics*. (Third edition, Kluwer Academic/Plenum Publisher, New York, 2000).